AIMS Mathematics, 8(4): 8185–8209.
DOI: 10.3934/math.2023414
Received: 29 November 2022
Revised: 01 January 2023
Accepted: 08 January 2023
Published: 01 February 2023

http://www.aimspress.com/journal/Math

Research article

Time fractional analysis of Casson fluid with application of novel hybrid fractional derivative operator

Aziz Ur Rehman[1], **Muhammad Bilal Riaz**[1,2,*], **Ilyas Khan**[3] **and Abdullah Mohamed**[4]

[1] Department of Mathematics, University of Management and Technology Lahore, Pakistan
[2] Faculty of Applied Physics and Mathematics, Gdansk University of Technology, 80-233 Gdansk, Poland
[3] Department of Mathematics, College of Science Al-Zulfi, Majmaah University, Al-Majmaah 11952, Saudi Arabia
[4] Research Centre, Future University in Egypt, New Cairo 11835, Egypt

* **Correspondence:** Email: Muhriaz@pg.edu.pl; Tel: +48729477868.

Abstract: A new approach is used to investigate the analytical solutions of the mathematical fractional Casson fluid model that is described by the Constant Proportional Caputo fractional operator having non-local and singular kernel near an infinitely vertical plate. The phenomenon has been expressed in terms of partial differential equations, and the governing equations were then transformed in non-dimensional form. For the sake of generalized memory effects, a new mathematical fractional model is formulated based on the newly introduced Constant Proportional Caputo fractional derivative operator. This fractional model has been solved analytically, and exact solutions for dimensionless velocity, concentration and energy equations are calculated in terms of Mittag-Leffler functions by employing the Laplace transformation method. For the physical significance of various system parameters such as α, β, Pr, Gr, Gm, Sc on velocity, temperature and concentration profiles, different graphs are demonstrated by Mathcad software. The Constant Proportional Caputo fractional parameter exhibited a retardation effect on momentum and energy profile, but it is visualized that for small values of Casson fluid parameter, the velocity profile is higher. Furthermore, to validated the acquired solutions, some limiting models such as the ordinary Newtonian model are recovered from the fractionalized model. Moreover, the graphical representations of the analytical solutions illustrated the main results of the present work. Also, from the literature, it is observed that to deriving analytical results from fractional fluid models developed by the various fractional operators is difficult, and this article contributes to answering the open problem of obtaining analytical solutions for the fractionalized fluid models.

Keywords: CPC derivative; analytical solution; special functions; system parameters
Mathematics Subject Classification: 33, 34, 76, 80

Abbreviations

Symbol	Quantity	Units
u	Fluid velocity	$\left(ms^{-1}\right)$
μ	Dynamic viscosity	$\left(Kgm^{-1}s^{-1}\right)$
T	Fluid temperature	(K)
C	Fluid concentration	$\left(Kgs^{-3}\right)$
υ	Kinematic coefficient of viscosity	$\left(m^2s^{-1}\right)$
Gr	Thermal Grashof number	$(-)$
Gm	Mass Grashof number	$(-)$
Dm	Mass diffusivity	$\left(m^2s^{-1}\right)$
g	Acceleration due to gravity	$\left(m.s^{-2}\right)$
T_w	Temperature of the plate	(K)
β_T	Volumetric coefficient of thermal expansion	$\left(K^{-1}\right)$
T_∞	Temperature of fluid far away from the plate	(K)
C_w	Concentration of the plate	$\left(Kgm^{-3}\right)$
β_C	Volumetric coefficient of mass expansion	$\left(m^3Kg^{-1}\right)$
C_∞	Concentration of fluid far away from the plate	$\left(Kgm^{-3}\right)$
ρ	Fluid density	$\left(Kgm^{-3}\right)$
β	Casson fluid parameter	$(-)$
σ	Electrical conductivity	$\left(sm^{-1}\right)$
Q_r	Radiative heat flux	$\left(Wm^{-2}\right)$
C_p	Specific heat at constant pressure	$\left(Jkg^{-1}K^{-1}\right)$
Pr	Prandtl number	$(-)$
Nr	Radiation parameter	$\left(Wm^{-1}K\right)$
Pr_0	Effective Prandtl number	$(-)$
s	Laplace transform parameter	$\left(s^{-1}\right)$
B_0	Imposed Magnetic field	$\left(Wm^{-2}\right)$
Q	Heat generation/absorption	$\left(JK^{-1}m^{-3}s^{-1}\right)$
M	Total Magnetic field	$(-)$
t	Time	(s)
k	Thermal conductivity of the fluid	$\left(Wm^{-2}K^{-1}\right)$
P	Pressure	$\left(Nm^{-2}\right)$
k_1	Coefficient of Rosseland absorption	$(-)$
σ_1	Stefan-Boltzmann constant	$\left(Wm^{-2}K^{-4}\right)$
α	Fractional parameter	$(-)$

1. Introduction

The process of heat and mass transfer has a great importance from the industrial point of view. Many researchers and scientists concentrate on this area. In modern technologies and various industrial fields, the non-Newtonian fluid theory has extensive impact because the Newtonian fluid model cannot express many flow characteristics. A non-Newtonian fluid obeys non-linear relationships between the rate of shear strain and the shear stress. The non-Newtonian fluid theory has significant utilization in modern engineering, especially in the petroleum industry for extracting crude oil from different petroleum productions. The properties of a Newtonian fluid in most cases are not valid, but scientists desire to model the complex behaviour of non-Newtonian fluid. The importance of non-Newtonian fluid has increased in the last few decades, specifically in the research field. The non-Newtonian fluids have numerous ever-increasing applications in industrial sectors, but some specific ones are mentioned here, such as: at large-scales reducing and enhancing heating/cooling systems, biochemical and process engineering, extrusion of molten plastic in industry, reducing oil pipeline friction, polymer processing, reducing fluid friction, well drilling, flow tracers, biological materials, biomedical flow analysis, plastic foam processing, lubrication processes, food processing industries, chemical processing, all emulsions, handling of muds, slurries and complex mixtures. Many researchers and scientists have focused on non-Newtonian fluid while considering different fluid geometries. Therefore, simulating and modelling the flow phenomena of non-Newtonian fluid has an important role in human life. Researchers investigated different non-Newtonian fluid models regarding physical and computational characteristics, such as the second grade model, viscoelastic model, power law model, Bingham plastic model, Jeffery model, Oldroyd-B fluid model, Brinkman type model, Casson model, Walters-B fluid model and Maxwell model [1–6]. Different fluid models in the literature have various characteristics or certain limitations. For instance, the second grade fluid model efficiently explains the elasticity but does not discuss the viscosity, and the power-law model describes the features of viscosity but fails to explain the impacts of elasticity. This motivates/attracts researchers and mathematicians towards the study of such complex fluids. Systematic analysis of such fluid flow models is important for theoretical studies and practical implementations in modern mechanization. Among such fluids, the Casson fluid has attracted special attention. It is also known as a shear-thinning liquid, which is the most common non-Newtonian fluid due to its extensive applications and substantial role in different fields, serving mechanical and chemical applications, bio engineering operations, metallurgy and especially in food processing industries. The Casson fluid model was initially proposed by Casson in 1959 with an aim to predict the flow regime of pigment-oil suspensions [7]. This structural model is based on the interaction of liquid and solid phases, which reveals yield stress. If the yield stress is larger than that of the applied shear force, then the liquid behaves like a solid. In contrast, if the yield stress is weaker than the shear stress, the liquid starts moving. Various materials of industrial applications, particularly those with multi-phase nature, including emulsions, slurries, foams and melting polymers, do not follow a linear shear stress and strain relationship. Honey, soup, jelly, china clay, tomato sauce, artificial fibers, synthetic lubricants, concentrated fruit juices, pharmaceutical chemicals, paints and coal some applications of such fluid. The Casson fluid model has numerous applications in cancer therapy. Blood also can be considered as a Casson fluid [8, 9] since it contains different materials like protein, globulin, fibrinogen in aqueous base plasma and red blood cells. The study of Casson fluid movement in the context of fluid

mechanics, was explored by several mathematicians, scientists, researchers and engineers, and it depends upon various situations. Khalid et al. [10] described unsteady, MHD natural convectional Casson fluid flow in a porous media. Bhatta charyya et al. [11] examined the magnetohydrodynamic flow of Casson fluid passing through and over a stretching/shrinking surface. Oka [12] studied for the first time Casson fluid movement through tubes. The two-dimensional peristaltic Casson fluid flow in a channel was investigated by Mernone et al. [13]. The induced magnetic field and chemical reaction on the movement of Casson fluid passing through porous media was discussed by Arthur et al. [14]. Khalil et al. [15] developed a flow field which was mathematically formulated and solved by using the Finite Element Method (FEM) in the presence of hybrid meshing; and modelling the non-Newtonian fluid in a cavity yields Rayleigh number, Casson fluid parameter and Darcy number. Lou et al. [16] investigated the momentum and thermal transportation of rotating dusty micro polar fluid flux with suspension of conducting dust particles across a stretched sheet. Ashraf et al. [17] established a unique computing exploration for steady magnetohydrodynamic convective streams of tangent hyperbolic nano-fluid travelling across a non-linearly elongating elastic surface with a variable thickness. Madhukesh [18] analysed the heat transference for two different boundary conditions, namely, Newtonian heating (NH) and constant wall temperature (CWT). The governing partial differential equations (PDEs) are reduced into ordinary differential equations (ODEs) by using appropriate similarity transformations. Then, they are numerically solved by using Runge-Kutta-Fehlberg's fourth fifth order (RKF-45) technique by adopting the shooting method. Bagh et al. [19] explored the significance of suction/injection for gravity modulation mixed convection in micro polar fluid flow due to an inclined sheet in the presence of magnetic field and thermal radiation. The mathematical modelling of the activation energy and binary chemical reaction system with six distinct types of nanoparticles, along with the magnetohydrodynamic effect, was studied by Raza et al. [20]. Mustafa et al. [21] analysed the heat transportation over a moving flat plate by using the method of homotopy analysis for unsteady flow of the boundary layer of the Casson model. The finite element analysis of the transient magnetohydrodynamic three-dimensional rotating flow of Maxwell and tangent hyperbolic nano-fluid flow past a bidirectional stretching sheet with the Cattaneo Christov heat flux model has been explored numerically by Bagh et al. [22]. Qureshi et al. [23] explored the heat transfer properties and flow features of an MHD hybrid nano-fluid due to the dispersion of polymer/CNT matrix nanocomposite material through orthogonal permeable disks with the impact of morphological nano-layer. Bagh et al. [24] studied the roles of volume fraction, Coriolis, and Lorentz forces on the dynamics of rotating water based silver tiny particles flow toward a continuously stretching sheet. Pramanik [25] performed a systematic study to analysed the effects of radiative thermal flux and porosity on mass and energy transfer.

Fractional calculus is an eminent mathematical field that is growing immensely due to enormous significance. It investigates the non integer order behaviour of integrals and derivatives as well as their applications and properties. The concept of differential calculus is old like classical calculus, In 1695, a new idea about fractional calculus was introduced when a letter from Leibniz to L′Hospital was written. This field attracted the attention of well known mathematicians, researchers and scientists that proposed and built different fractional integrals and fractional derivatives. The researchers faced too much difficulties to developed a real physical phenomenon by employing the traditional calculus techniques, and the fractional differential equations have great importance for mathematicians and researchers. It has been used in investigating numerous physical models in different scientific fields,

such as biology, physics, chemistry, acoustic waves, finance, control theory, fractal dynamics, signal processing, hydromagnetic waves, diffusion reaction process, anomalous transport, fluid flow problems, engineering processes, oscillation, dynamical processes and many other disciplines. The main reason for exploring the numerical or exact solutions is due to their significance in daily life. To gain the numerical or exact solutions, researchers and mathematicians have implemented numerous techniques. These include the unified method [26], multi step approach [27, 28], Riccati-Bernoulli sub-ordinary differential equation Sub-ODE technique (RBSODET) [29], reproducing the kernel Hilbert space method [30, 31], simple equation modification method [32], residual power series method [33] and several others [34–36]. Due to the advancement in the field of fractional calculus, scientists have suggested a couple of new techniques to interpret and establish real world problem solutions using the theory of fractional calculus. To interpret and model phenomena in different fields of science, such as electric circuit models, fractal rheological models and fractal growth of populations models, several fractional operators have singular kernels. However, several with non-singular kernels have been developed, which is an important tool to analyse the rheological behaviour of the physical models in fractional calculus. In the literature, many researchers work a lot in this shining field of mathematics to analysed the fractional fluid models and derived various interesting results that are very helpful for engineers and scientists to compare their experimental results get from the govern partial differential equations with the analytical results obtained using different mathematical techniques and tools from fractional form of the non-Newtonian fluid models. Marchaud Caputo and Riemann-Liouville developed fractional integrals and described a new concept of fractional derivatives operators, that are based on singular kernels, but these fractional models have some drawbacks due to the singular kernels and face many difficulties during the modelling process. To overcome this hurdle that occurs with singular kernel fractional models , a new set of fractional operators have been presented that are based on non-singular kernels, such as the Prabhakar fractional derivative; Caputo-Fabrizio, Yang Abdel Cattani fractional, Atangana-Baleanu fractional operators; and a few others, for reference [37–43]. These fractional operators have different types of non-singular kernels, including Rabotnov exponential function, Exponential kernels and Mittag-Leffler functions.

In a previous investigation, Ndolane Sene et al. [44] discussed the flow of Casson fluid with a Caputo fractional model without considering the effect of mass diffusion, and they computed analytically the presented model by using integral Laplace transformation, because it has efficient applications for non-uniform boundary conditions. However a fractional Casson fluid model developed by the CPC fractional operator, along with the set of symmetric conditions for mass, energy and velocity, saturated in porous media, has not yet been investigated or published in the literature. To fill this gap, a new fractional Casson model is developed under effectively applied conditions for concentration, velocity field and temperature distribution. Further, in the presented model, a new fractional operator is employed to fractionalized the diffusion, velocity and energy equations together with the set of same conditions, applying the definition of a new fractional derivative operator, the Constant Proportional Caputo operator, having non-local and singular kernel. Owning to such interest, for better rheology of Casson fluid, developed a fractional model by employing the new definition of the Constant Proportional Caputo fractional derivative operator that describes the generalized memory effects. For seeking exact solution expressions in terms of Mittag-Leffler functions, for velocity and temperature, the Laplace integral transformation method is

used to solve the fractional model. For physical analysis, the influences of parameters like CPC fractional order α, thermal Grashof number Gr, Casson fluid parameter β, Prandtl number Pr, Schmidt number Sc and mass Grashof number Gm are portrayed graphically by using Mathcad software. Furthermore, for validation of the current result, limiting models such as the fractional Newtonian model are obtained from the CPC fractional Casson model.

2. Mathematical model

Consider the Casson fluid flow over an infinite erected plate, having infinite length, that is embedded in a porous medium. The plate is considered to be at $\phi = 0$, and the fluid flow is restrained to $\phi > 0$, in the direction that is along the plate (as exhibited in Figure 1). We consider the following key assumptions that are supposed to govern the Casson fluid flow model:

- The flow is unidirectional and one-dimensional.
- To omit the impact of an induction magnetic field, Reynolds number is considered small enough.
- A uniform magnetic force of lines with magnitude B_0 is imposed in the direction which is perpendicular to the plate.
- It is considered that no electric force is applied to avoid the polarization influence of fluid.
- Suppose the Q_r (radiative heat flux) is negligible which is in the direction that is too the plate corresponding to the radiative thermal flux that is in the normal direction of the plate.
- The energy equation without viscous dissipation term is considered.

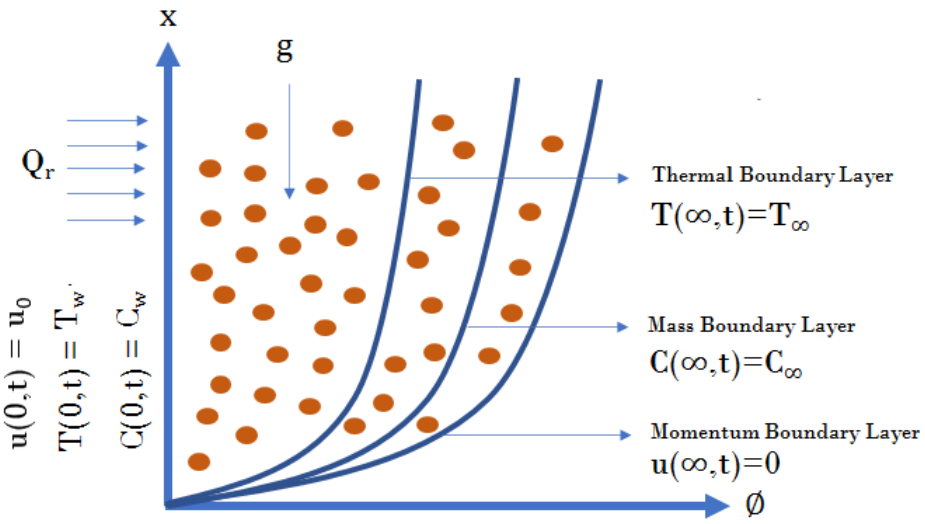

Figure 1. Geometry of the flow model.

The set of Maxwell equations that is used to represent the magnetic field relations is written as follows:

$$divM = 0, \quad CurlE = -\frac{\partial M}{\partial t}, \quad CurlM = J\mu_m, \tag{2.1}$$

where $\boldsymbol{J}$ represents the current density, μ_m represents the magnetic permeability, and $\boldsymbol{E}$ represents the electric field. Furthermore, $\boldsymbol{M}$ is the sum of $\boldsymbol{B_0}$(imposed magnetic field) and $\boldsymbol{M_0}$ (induced magnetic

field), which is neglected in this case. From Ohm's law,

$$\boldsymbol{J} = (\boldsymbol{U} \times \boldsymbol{M} + \boldsymbol{E})\sigma, \tag{2.2}$$

where U denotes the fluid velocity, and σ denotes the electrical conductivity. Also, suppose that the small Reynolds number gives the following expression:

$$(\boldsymbol{J} \times \boldsymbol{M})\frac{1}{\rho} = ((\boldsymbol{U} \times \boldsymbol{B_0}) \times \boldsymbol{B_0})\frac{\sigma}{\rho} = -\frac{\sigma u \boldsymbol{B_0}^2}{\rho}. \tag{2.3}$$

The rheological model is expressed as the following Cauchy stress tensor [45, 46]:

$$t_{xy} = \begin{cases} 2(\mu_t + \frac{P_\lambda}{\sqrt{2\pi}})e_{xy}, & \pi > \pi_z \\ 2(\mu_t + \frac{P_\lambda}{\sqrt{2\pi_z}})e_{xy}, & \pi < \pi_z \end{cases}, \tag{2.4}$$

where μ_t denotes the plastic dynamic viscosity, P_λ represents the yield stress, π denotes the self product of the component deformation rate, e_{xy} represents the deformation rate at $(x, y)^{th}$ component, and π_z is the critical value of the earlier mentioned product that depends upon the non-Newtonian model. Initially, for time $t = 0$, the fluid and plate both are in the static mode, having ambient temperature T_∞ and concentration C_∞. Later, when time $t = 0^+$, the wall temperature is $T(0, t) = T_w$, and the concentration $C(0, t) = C_w$, $u(\phi, t)$ is taken as the velocity component along the x-axis with u_0 as the characteristic velocity. Further, the velocity field satisfies the equation of continuity in the presence of these factors. By considering all of the above mentioned assumptions, the following principal equations for Casson fluid velocity under Boussinesq's approximation, for concentration and energy transfer are obtained as in [47, 48].

The momentum, energy and concentration equations, along with Fourier's thermal flux Law and Fick's Law,are given below:

The momentum equation:

$$\frac{\partial u(\phi, t)}{\partial t} = \upsilon\left(1 + \frac{1}{\beta}\right)\frac{\partial^2 u(\phi, t)}{\partial \phi^2} + g\beta_T\left(T(\phi, t) - T_\infty\right) + g\beta_C\left(C(\phi, t) - C_\infty\right). \tag{2.5}$$

The energy equation:

$$\frac{\partial T(\phi, t)}{\partial t} = -\frac{1}{\rho C_p}\frac{\partial q(\phi, t)}{\partial \phi} - \frac{\partial Q_r}{\partial \phi}, \quad \left[Q_r = -\frac{4\sigma_1}{3k_1}\frac{\partial T^4}{\partial \phi}; T^4 \approx 4T_\infty^3 T - 3T_\infty^4\right]. \tag{2.6}$$

Fourier's Law:

$$q(\phi, t) = -k\frac{\partial T(\phi, t)}{\partial \phi}. \tag{2.7}$$

The diffusion equation:

$$\frac{\partial C(\phi, t)}{\partial t} = -\frac{\partial \chi(\phi, t)}{\partial \phi}. \tag{2.8}$$

Fick's Law:

$$\chi(\phi,t) = -D_m \frac{\partial C(\phi,t)}{\partial \phi}, \tag{2.9}$$

with initial and boundary conditions are

$$\begin{aligned} &u(\phi,0) = 0, \quad T(\phi,0) = T_\infty, \quad C(\phi,0) = C_\infty, \quad \phi > 0, \\ &u(0,t) = u_0, \quad T(0,t) = T_w, \quad C(0,t) = C_w, \quad t > 0, \\ &u(\phi,t) \to 0, \quad T(\phi,t) \to T_\infty, \quad C(\phi,t) \to C_\infty \quad as \quad \phi \to \infty. \end{aligned} \tag{2.10}$$

To reduce the number of involved parameters, we have introduced the following new set of unit-free quantities:

$$\begin{aligned} &t^* = \frac{u_0^2 t}{\upsilon}, \quad \phi^* = \frac{u_0 \phi}{\upsilon}, \quad u^* = \frac{u}{u_0}, \quad \upsilon = \frac{\mu}{\rho}, \quad T^* = \frac{T - T_\infty}{T_w - T_\infty}, \quad C^* = \frac{C - C_\infty}{C_w - C_\infty}, \\ &q^* = \frac{q}{q_0}, \quad \chi^* = \frac{\chi}{\chi_0}, \quad q_0 = \frac{k(T_w - T_\infty)u_0}{\upsilon}, \quad \chi_0 = \frac{D_m(C_w - C_\infty)u_0}{\upsilon}, \quad Sc = \frac{\upsilon}{D_m}, \\ &Gr = \frac{g\upsilon\beta_T(T_w - T_\infty)}{u_0^3}, \quad Gm = \frac{g\upsilon\beta_C(C_w - C_\infty)}{u_0^3}, \quad Pr = \frac{\mu C_p}{k}, \\ &N_r = \frac{16\sigma_1 T_\infty^3}{3kk_1}, \quad Pr_0 = \frac{P_r}{1 + N_r}, \quad \frac{1}{\lambda} = \left(1 + \frac{1}{\beta}\right). \end{aligned} \tag{2.11}$$

When substituting Eq (2.11) into Eqs (2.5), (2.6) and (2.8), and dropping the asterisk $*$ from newly obtained equations, we have the dimensionless governing system of partial differential equations of the considered model as follows:

$$\frac{\partial u(\phi,t)}{\partial t} = \frac{1}{\lambda}\frac{\partial^2 u(\phi,t)}{\partial \phi^2} + GrT(\phi,t) + GmC(\phi,t), \tag{2.12}$$

$$\frac{\partial T(\phi,t)}{\partial t} = -\frac{1}{Pr_0}\frac{\partial q(\phi,t)}{\partial \phi}, \tag{2.13}$$

$$q(\phi,t) = -\frac{\partial T(\phi,t)}{\partial \phi}, \tag{2.14}$$

$$\frac{\partial C(\phi,t)}{\partial t} = -\frac{1}{Sc}\frac{\partial \chi(\phi,t)}{\partial \phi}, \tag{2.15}$$

$$\chi(\phi,t) = -\frac{\partial C(\phi,t)}{\partial \phi}. \tag{2.16}$$

The analogous initial and boundary conditions when applying the new quantities mentioned in Eq (2.11) for non-dimensionalization are

$$u(\phi,0) = 0, \quad T(\phi,0) = 0, \quad C(\phi,0) = 0, \quad for \quad \phi > 0, \tag{2.17}$$

$$u(0,t) = 1, \quad T(0,t) = 1, \quad C(0,t) = 1, \quad for \quad t > 0, \tag{2.18}$$

$$u(\phi,t) \to 0, \quad T(\phi,t) \to 0, \quad C(\phi,t) \to 0 \quad as \quad \phi \to \infty. \tag{2.19}$$

3. Preliminaries

The Constant Proportional Caputo (CPC) hybrid fractional operator used in this work was developed recently by Dumitru et al. [49]. This newly developed fractional operator is a linear combination of two fractional operators, namely, the Constant proportional and Caputo fractional derivative operators, so it is also called a hybrid fractional operator. The CPC-fractional derivative operator of order α is described as

$$ {}^{CPC}D_t^{\alpha} f(\psi, t) = \frac{1}{\Gamma(1-\alpha)} \int_0^t (k_1(\alpha) f(\psi, \tau) + k_0(\alpha) \frac{\partial f(\psi, \tau)}{\partial \tau})(t-\tau)^{-\alpha} d\tau, \quad 0 < \alpha < 1. \tag{3.1} $$

The Laplace transformation of the Constant proportional-Caputo hybrid time fractional operator is written as:

$$ L\left({}^{CPC}D_t^{\alpha} f(\psi, t)\right) = \left[\frac{k_1(\alpha)}{s} + k_0(\alpha)\right] s^{\alpha} L(f(\psi, t)) - k_0(\alpha) s^{\alpha-1} f(\psi, 0), \tag{3.2} $$

where α is used to represent the fractional parameter, and Laplace transform parameter is denoted by s. Here, the functions k_0 and k_1 depend only on parameter α.

4. Solution of the problem

In the present article, introducing a novel mathematical model named as Constant Proportional Caputo fractional operator which generalized the thermal memory effects. The time-fractional Casson fluid equations for velocity, energy and concentration based on Constant Proportional Caputo derivative operator are given as:

$$ {}^{CPC}D_t^{\alpha} u(\phi, t) = \frac{1}{\lambda} \frac{\partial^2 u(\phi, t)}{\partial \phi^2} + GrT(\phi, t) + GmC(\phi, t), \tag{4.1} $$

$$ {}^{CPC}D_t^{\alpha} T(\phi, t) = \frac{1}{Pr_0} \frac{\partial^2 T(\phi, t)}{\partial \phi^2}, \tag{4.2} $$

$$ {}^{CPC}D_t^{\alpha} C(\phi, t) = \frac{1}{Sc} \frac{\partial^2 C(\phi, t)}{\partial \phi^2}, \tag{4.3} $$

where, ${}^{CPC}D_t^{\alpha}(.,.)$ represents the Constant Proportional-Caputo hybrid fractional operator, with detailed discussion of properties in [49].

4.1. Temperature equation solution by using CPC derivative operator

To derive the solution for energy, Eq (4.2), with appropriate non-dimensional conditions Eqs (2.17)–(2.19), we employ the technique of Laplace transformation in view of Eq (3.2) as follows:

$$ Pr_0 \left(\left[\frac{k_1(\alpha)}{s} + k_0(\alpha)\right] s^{\alpha} \bar{T}(\phi, s) - k_0(\alpha) s^{\alpha-1} \bar{T}(\phi, 0) \right) = \frac{d^2 \bar{T}(\phi, s)}{d\phi^2}, \tag{4.4} $$

with

$$\bar{T}(\phi,0)=0,\quad \bar{T}(0,s)=\frac{1}{s}\quad and\quad \bar{T}(\phi,s)\to 0\quad as\quad \phi\to\infty. \tag{4.5}$$

The definition of Laplace integral transformation of any function $X(\phi,t)$, denoted by $\bar{X}(\phi,s)$, is expressed mathematically as:

$$\bar{X}(\phi,s)=\int_0^\infty X(\phi,t)e^{-st}dt.$$

The energy solution for Eq (4.4) is written in the form:

$$\bar{T}(\phi,s)=e_1e^{-\phi\sqrt{Pr_0\left[\frac{k_1(\alpha)}{s}+k_0(\alpha)\right]s^\alpha}}+e_2e^{\phi\sqrt{Pr_0\left[\frac{k_1(\alpha)}{s}+k_0(\alpha)\right]s^\alpha}}. \tag{4.6}$$

The temperature solution of Eq (4.6) which satisfies the boundary conditions Eq (4.5) is given by

$$\bar{T}(\phi,s)=\frac{1}{s}e^{-\phi\sqrt{Pr_0\left[\frac{k_1(\alpha)}{s}+k_0(\alpha)\right]s^\alpha}}. \tag{4.7}$$

We write Eq (4.7) in series equivalent form, because from the above form of the equation, it is difficult to compute the Laplace inverse more precisely. By using the Taylor series expansion for the exponential function, it becomes:

$$\bar{T}(\phi,s)=\sum_{n=0}^{\infty}\frac{(-\phi)^n(Pr_0k_0(\alpha))^{\frac{n}{2}}}{n!}.\frac{1}{s^{1-\frac{n\alpha}{2}}\left(1+\frac{k_1(\alpha)}{k_0(\alpha)}s^{-1}\right)^{-\frac{n}{2}}}. \tag{4.8}$$

The required temperature field solution is given by the inverse Laplace transform of Eq (4.8):

$$T(\phi,t)=\sum_{n=0}^{\infty}\frac{(-\phi)^n(Pr_0k_0(\alpha))^{\frac{n}{2}}}{n!}t^{-\frac{n\alpha}{2}}E^{\frac{-n}{2}}_{1,1-\frac{n\alpha}{2}}\left(-\frac{k_1(\alpha)}{k_0(\alpha)}t\right). \tag{4.9}$$

Moreover, the rate of heat transfer can be determined from the Nusselt number (Nu), defined as

$$\begin{aligned}
Nu&=-\frac{\partial T(\phi,t)}{\partial\phi}\Big|_{\phi=0}\\
&=-\frac{\partial}{\partial\phi}L^{-1}\left\{\bar{T}(\phi,s)\right\}\Big|_{\phi=0}\\
&=-L^{-1}\left\{\frac{\partial\bar{T}(\phi,s)}{\partial\phi}\Big|_{\phi=0}\right\}\\
&=L^{-1}\left\{(Pr_0k_0(\alpha))^{\frac{1}{2}}\frac{1}{s^{1-\frac{\alpha}{2}}\left(1+\frac{k_1(\alpha)}{k_0(\alpha)}s^{-1}\right)^{-\frac{1}{2}}}\right\}\\
&=(Pr_0k_0(\alpha))^{\frac{1}{2}}t^{-\frac{\alpha}{2}}E^{\frac{-1}{2}}_{1,1-\frac{\alpha}{2}}\left(-\frac{k_1(\alpha)}{k_0(\alpha)}t\right),
\end{aligned} \tag{4.10}$$

by using

$$L^{-1}\left\{\frac{s^{-\beta}}{(1-\wp s^{-\alpha})^\gamma}\right\}=t^{\beta-1}E^\gamma_{\alpha,\beta}(\wp t^\alpha).$$

4.2. Diffusion equation solution by using CPC derivative operator

To derive the solution for mass, Eq (4.3), with appropriate non-dimensional conditions Eqs (2.17)–(2.19), we employ the technique of Laplace transformation in view of Eq (3.2) as follows:

$$Sc\left[\frac{k_1(\alpha)}{s}+k_0(\alpha)\right]s^{\alpha}\bar{C}(\phi,s)-k_0(\alpha)s^{\alpha-1}\bar{C}(\phi,0)=\frac{\partial^2\bar{C}(\phi,s)}{\partial\phi^2}, \tag{4.11}$$

with

$$\bar{C}(\phi,0)=0,\quad \bar{C}(0,s)=\frac{1}{s}\quad and\quad \bar{C}(\phi,s)\to 0\quad as\quad \phi\to\infty. \tag{4.12}$$

The solution for the concentration fractional differential equation Eq (4.11) is obtained as:

$$\bar{C}(\phi,s)=e_3e^{-\phi\sqrt{Sc\left[\frac{k_1(\alpha)}{s}+k_0(\alpha)\right]s^{\alpha}}}+e_4e^{\phi\sqrt{Sc\left[\frac{k_1(\alpha)}{s}+k_0(\alpha)\right]s^{\alpha}}}. \tag{4.13}$$

The concentration solution of Eq (4.13) which satisfies the boundary conditions Eq (4.5) is given by

$$\bar{C}(\phi,s)=\frac{1}{s}e^{-\phi\sqrt{Sc\left[\frac{k_1(\alpha)}{s}+k_0(\alpha)\right]s^{\alpha}}}. \tag{4.14}$$

We write Eq (4.14) in series equivalent form, because from the above form of the equation, it is difficult to compute the Laplace inverse more precisely. By using the Taylor series expansion for the exponential function, it becomes:

$$\bar{C}(\phi,s)=\sum_{n=0}^{\infty}\frac{(-\phi)^n(Sck_0(\alpha))^{\frac{n}{2}}}{n!}.\frac{1}{s^{1-\frac{n\alpha}{2}}\left(1+\frac{k_1(\alpha)}{k_0(\alpha)}s^{-1}\right)^{-\frac{n}{2}}}. \tag{4.15}$$

The required concentration solution is given by the inverse Laplace transform of the above Eq (4.15):

$$C(\phi,t)=\sum_{n=0}^{\infty}\frac{(-\phi)^n(Sck_0(\alpha))^{\frac{n}{2}}}{n!}t^{-\frac{n\alpha}{2}}E^{\frac{-n}{2}}_{1,1-\frac{n\alpha}{2}}\left(-\frac{k_1(\alpha)}{k_0(\alpha)}t\right). \tag{4.16}$$

The mass transfer rate, known as Sherwood number (Sh), is defined as

$$\begin{aligned}
Sh&=-\frac{\partial C(\phi,t)}{\partial\phi}\Big|_{\phi=0}\\
&=-\frac{\partial}{\partial\phi}L^{-1}\left\{\bar{C}(\phi,s)\right\}\Big|_{\phi=0}\\
&=-L^{-1}\left\{\frac{\partial\bar{C}(\phi,s)}{\partial\phi}\Big|_{\phi=0}\right\}\\
&=L^{-1}\left\{(Sck_0(\alpha))^{\frac{1}{2}}\frac{1}{s^{1-\frac{\alpha}{2}}\left(1+\frac{k_1(\alpha)}{k_0(\alpha)}s^{-1}\right)^{-\frac{1}{2}}}\right\}\\
&=(Sck_0(\alpha))^{\frac{1}{2}}t^{-\frac{\alpha}{2}}E^{\frac{-1}{2}}_{1,1-\frac{\alpha}{2}}\left(-\frac{k_1(\alpha)}{k_0(\alpha)}t\right).
\end{aligned} \tag{4.17}$$

4.3. Velocity field solution by using CPC derivative operator

To derive the solution for velocity field, Eq (4.1), with appropriate non-dimensional conditions Eqs (2.17)–(2.19), we employ the Laplace transformation method in view of Eq (3.2) as follows:

$$\lambda\left[\frac{k_1(\alpha)}{s}+k_0(\alpha)\right]s^{\alpha}\bar{u}(\phi,s)-k_0(\alpha)s^{\alpha-1}\bar{u}(\phi,0)=\frac{d^2\bar{u}(\phi,s)}{d\phi^2}+\lambda Gr\bar{T}(\phi,s)+\lambda Gm\bar{C}(\phi,s), \tag{4.18}$$

with transformed conditions are:

$$\bar{u}(\phi,0)=0,\quad \bar{u}(0,s)=\frac{1}{s}\quad and\quad \bar{u}(\phi,s)\to 0\quad as\quad \phi\to\infty. \tag{4.19}$$

The solution for the velocity fractional differential equation Eq (4.18), together with $\bar{T}(\phi,s)$ and $\bar{C}(\phi,s)$ are taken from Eqs (4.8) and (4.15), is written as:

$$\begin{aligned}\bar{u}(\phi,s)=\;&e_5e^{-\phi\sqrt{\lambda\left[\frac{k_1(\alpha)}{s}+k_0(\alpha)\right]s^{\alpha}}}+e_6e^{\phi\sqrt{\lambda\left[\frac{k_1(\alpha)}{s}+k_0(\alpha)\right]s^{\alpha}}}\\&+\left(\frac{\lambda Gr}{\lambda-Pr_0}\right)\left(\frac{1}{s\lambda\left[\frac{k_1(\alpha)}{s}+k_0(\alpha)\right]s^{\alpha}}\right)e^{-\phi\sqrt{Pr_0\left[\frac{k_1(\alpha)}{s}+k_0(\alpha)\right]s^{\alpha}}}\\&+\left(\frac{\lambda Gm}{\lambda-Sc}\right)\left(\frac{1}{s\lambda\left[\frac{k_1(\alpha)}{s}+k_0(\alpha)\right]s^{\alpha}}\right)e^{-\phi\sqrt{Sc\left[\frac{k_1(\alpha)}{s}+k_0(\alpha)\right].s^{\alpha}}}.\end{aligned} \tag{4.20}$$

The velocity solution of Eq (4.20) which satisfies the boundary conditions Eq (4.19) is given by

$$\begin{aligned}\bar{u}(\phi,s)=\;&\frac{1}{s}e^{-\phi\sqrt{\lambda\left[\frac{k_1(\alpha)}{s}+k_0(\alpha)\right]s^{\alpha}}}\\&+\left(\frac{\lambda Gr}{\lambda-Pr_0}\right)\left(\frac{1}{s\lambda\left[\frac{k_1(\alpha)}{s}+k_0(\alpha)\right]s^{\alpha}}\right)\left[e^{-\phi\sqrt{Pr_0\left[\frac{k_1(\alpha)}{s}+k_0(\alpha)\right]s^{\alpha}}}-e^{-\phi\sqrt{\lambda\left[\frac{k_1(\alpha)}{s}+k_0(\alpha)\right]s^{\alpha}}}\right]\\&+\left(\frac{\lambda Gm}{\lambda-Sc}\right)\left(\frac{1}{s\lambda\left[\frac{k_1(\alpha)}{s}+k_0(\alpha)\right]s^{\alpha}}\right)\left[e^{-\phi\sqrt{Sc\left[\frac{k_1(\alpha)}{s}+k_0(\alpha)\right].s^{\alpha}}}-e^{-\phi\sqrt{\lambda\left[\frac{k_1(\alpha)}{s}+k_0(\alpha)\right]s^{\alpha}}}\right].\end{aligned} \tag{4.21}$$

Equation (4.21) is written in a new way to compute its inverse easily, which implies that

$$\begin{aligned}\bar{u}(\phi,s)=\;&\bar{u}_1(\phi,s)+\left(\frac{\lambda Gr}{\lambda-Pr_0}\right)\bar{u}_2(\phi,s)\left[\bar{T}(\phi,s)-\bar{u}_1(\phi,s)\right]\\&+\left(\frac{\lambda Gm}{\lambda-Sc}\right)\bar{u}_2(\phi,s)\left[\bar{C}(\phi,s)-\bar{u}_1(\phi,s)\right].\end{aligned} \tag{4.22}$$

Computing the velocity solution using the Laplace inverse transformation, the required velocity solution is given by

$$\begin{aligned}u(\phi,t)=\;&u_1(\phi,t)+\left(\frac{\lambda Gr}{\lambda-Pr_0}\right)u_2(\phi,t)*\left[T(\phi,t)-u_1(\phi,t)\right]\\&+\left(\frac{\lambda Gm}{\lambda-Sc}\right)u_2(\phi,t)*\left[C(\phi,t)-u_1(\phi,t)\right],\end{aligned} \tag{4.23}$$

where

$$u_1(\phi,t) = L^{-1}\{\bar{u}_1(\phi,s)\} = L^{-1}\left\{\frac{1}{s}e^{-\phi\sqrt{\lambda\left[\frac{k_1(\alpha)}{s}+k_0(\alpha)\right]s^\alpha}}\right\}$$
$$= L^{-1}\left\{\sum_{n=0}^{\infty}\frac{(-\phi)^n(\lambda k_0(\alpha))^{\frac{n}{2}}}{n!}.\frac{1}{s^{1-\frac{n\alpha}{2}}\left(1+\frac{k_1(\alpha)}{k_0(\alpha)}s^{-1}\right)^{-\frac{n}{2}}}\right\}$$
$$= \sum_{n=0}^{\infty}\frac{(-\phi)^n(\lambda k_0(\alpha))^{\frac{n}{2}}}{n!}t^{\frac{n\alpha}{2}}E^{\frac{-n}{2}}_{1,1-\frac{n\alpha}{2}}\left(-\frac{k_1(\alpha)}{k_0(\alpha)}t\right)$$
$$u_2(\phi,t) = L^{-1}\{\bar{u}_2(\phi,s)\} = L^{-1}\left\{\frac{1}{s^\alpha\left[\frac{k_1(\alpha)}{s}+k_0(\alpha)\right]}\right\}$$
$$= \frac{1}{k_0(\alpha)}t^{\alpha-1}E_{1,\alpha}\left(-\frac{k_1(\alpha)}{k_0(\alpha)}t\right).$$

The relation for skin friction (Cf) (wall shear stress) is presented as

$$Cf = \left(1+\frac{1}{\beta}\right)\frac{\partial u(\phi,t)}{\partial\phi}\Big|_{\phi=0}$$
$$= \left(1+\frac{1}{\beta}\right)\frac{\partial}{\partial\phi}L^{-1}\{\bar{u}(\phi,s)\}\Big|_{\phi=0}$$
$$= \left(1+\frac{1}{\beta}\right)L^{-1}\left\{\frac{\partial\bar{u}(\phi,s)}{\partial\phi}\Big|_{\phi=0}\right\}, \tag{4.24}$$

with

$$\frac{\partial\bar{u}(\phi,s)}{\partial\phi}\Big|_{\phi=0} = -\frac{1}{s}\sqrt{\lambda\left[\frac{k_1(\alpha)}{s}+k_0(\alpha)\right]s^\alpha}$$
$$+\left(\frac{\lambda Gr}{\lambda-Pr_0}\right)\left(\frac{1}{s\lambda\left[\frac{k_1(\alpha)}{s}+k_0(\alpha)\right]s^\alpha}\right)\left[-\sqrt{Pr_0\left[\frac{k_1(\alpha)}{s}+k_0(\alpha)\right]s^\alpha}+\sqrt{\lambda\left[\frac{k_1(\alpha)}{s}+k_0(\alpha)\right]s^\alpha}\right]$$
$$+\left(\frac{\lambda Gm}{\lambda-Sc}\right)\left(\frac{1}{s\lambda\left[\frac{k_1(\alpha)}{s}+k_0(\alpha)\right]s^\alpha}\right)\left[-\sqrt{Sc\left[\frac{k_1(\alpha)}{s}+k_0(\alpha)\right].s^\alpha}+\sqrt{\lambda\left[\frac{k_1(\alpha)}{s}+k_0(\alpha)\right]s^\alpha}\right]. \tag{4.25}$$

After applying the Laplace inverse transformation of Eq (4.25), the result is obtained as

$$L^{-1}\left\{\frac{\partial\bar{u}(\phi,s)}{\partial\phi}\Big|_{\phi=0}\right\}$$
$$= -(\lambda k_0(\alpha))^{\frac{1}{2}}t^{-\frac{\alpha}{2}}E^{\frac{-1}{2}}_{1,1-\frac{\alpha}{2}}\left(-\frac{k_1(\alpha)}{k_0(\alpha)}t\right)$$
$$+\left(\frac{Gr}{\lambda-Pr_0}\right)\left[\sqrt{\lambda}(k_0(\alpha))^{-\frac{1}{2}}t^{\frac{\alpha}{2}}E^{\frac{1}{2}}_{1,1+\frac{\alpha}{2}}\left(-\frac{k_1(\alpha)}{k_0(\alpha)}t\right)-\sqrt{Pr_0}(k_0(\alpha))^{-\frac{1}{2}}t^{\frac{\alpha}{2}}E^{\frac{1}{2}}_{1,1+\frac{\alpha}{2}}\left(-\frac{k_1(\alpha)}{k_0(\alpha)}t\right)\right]$$

$$+\left(\frac{Gm}{\lambda - Sc}\right)\left[\sqrt{\lambda}(k_0(\alpha))^{-\frac{1}{2}}t^{\frac{\alpha}{2}}E^{\frac{1}{2}}_{1,1+\frac{\alpha}{2}}\left(-\frac{k_1(\alpha)}{k_0(\alpha)}t\right) - \sqrt{Sc}(k_0(\alpha))^{-\frac{1}{2}}t^{\frac{\alpha}{2}}E^{\frac{1}{2}}_{1,1+\frac{\alpha}{2}}\left(-\frac{k_1(\alpha)}{k_0(\alpha)}t\right)\right]. \tag{4.26}$$

It can also be written in more precise form as

$$\begin{aligned} L^{-1}\left\{\frac{\partial\bar{u}(\phi,s)}{\partial\phi}\Big|_{\phi=0}\right\} = &-(\lambda k_0(\alpha))^{\frac{1}{2}}t^{-\frac{\alpha}{2}}E^{\frac{-1}{2}}_{1,1-\frac{\alpha}{2}}\left(-\frac{k_1(\alpha)}{k_0(\alpha)}t\right) \\ &+(k_0(\alpha))^{-\frac{1}{2}}t^{\frac{\alpha}{2}}E^{\frac{1}{2}}_{1,1+\frac{\alpha}{2}}\left(-\frac{k_1(\alpha)}{k_0(\alpha)}t\right)\left[\left(\frac{Gr}{\sqrt{\lambda}+\sqrt{Pr_0}}\right)+\left(\frac{Gm}{\sqrt{\lambda}+\sqrt{Sc}}\right)\right]. \end{aligned} \tag{4.27}$$

5. Limiting models

When the Casson fluid parameter β is very large, i.e, $\frac{1}{\beta} \to 0$, then the behaviour of the non-Newtonian fluid reduces to that of Newtonian fluid, and the velocity of Eq (4.21) turns out as

$$\begin{aligned} \bar{u}(\phi,s) = &\frac{1}{s}e^{-\phi\sqrt{\left[\frac{k_1(\alpha)}{s}+k_0(\alpha)\right]s^{\alpha}}} \\ &+\left(\frac{Gr}{1-Pr_0}\right)\left(\frac{1}{s\left[\frac{k_1(\alpha)}{s}+k_0(\alpha)\right]s^{\alpha}}\right)\left[e^{-\phi\sqrt{Pr_0\left[\frac{k_1(\alpha)}{s}+k_0(\alpha)\right]s^{\alpha}}} - e^{-\phi\sqrt{\left[\frac{k_1(\alpha)}{s}+k_0(\alpha)\right]s^{\alpha}}}\right] \\ &+\left(\frac{Gm}{1-Sc}\right)\left(\frac{1}{s\left[\frac{k_1(\alpha)}{s}+k_0(\alpha)\right]s^{\alpha}}\right)\left[e^{-\phi\sqrt{Sc\left[\frac{k_1(\alpha)}{s}+k_0(\alpha)\right].s^{\alpha}}} - e^{-\phi\sqrt{\left[\frac{k_1(\alpha)}{s}+k_0(\alpha)\right]s^{\alpha}}}\right]. \end{aligned} \tag{5.1}$$

Equation (5.1) is written in a new way to compute its inverse easily, which implies that

$$\begin{aligned} \bar{u}(\phi,s) = &\bar{u}_3(\phi,s)+\left(\frac{Gr}{1-Pr_0}\right)\bar{u}_4(\phi,s)\left[\bar{T}(\phi,s)-\bar{u}_3(\phi,s)\right] \\ &+\left(\frac{Gm}{1-Sc}\right)\bar{u}_4(\phi,s)\left[\bar{C}(\phi,s)-\bar{u}_3(\phi,s)\right]. \end{aligned} \tag{5.2}$$

Computing the velocity solution using the Laplace inverse transformation, the required velocity solution is given by

$$\begin{aligned} u(\phi,t) = &u_3(\phi,t)+\left(\frac{Gr}{1-Pr_0}\right)u_4(\phi,t)*\left[T(\phi,t)-u_3(\phi,t)\right] \\ &+\left(\frac{Gm}{1-Sc}\right)u_4(\phi,t)*\left[C(\phi,t)-u_3(\phi,t)\right], \end{aligned} \tag{5.3}$$

where

$$\begin{aligned} u_3(\phi,t) = L^{-1}\left\{\bar{u}_3(\phi,s)\right\} &= L^{-1}\left\{\frac{1}{s}e^{-\phi\sqrt{\left[\frac{k_1(\alpha)}{s}+k_0(\alpha)\right]s^{\alpha}}}\right\} \\ &= L^{-1}\left\{\sum_{n=0}^{\infty}\frac{(-\phi)^n(k_0(\alpha))^{\frac{n}{2}}}{n!}.\frac{1}{s^{1-\frac{n\alpha}{2}}\left(1+\frac{k_1(\alpha)}{k_0(\alpha)}s^{-1}\right)^{-\frac{n}{2}}}\right\} \end{aligned}$$

$$= \sum_{n=0}^{\infty} \frac{(-\phi)^n (k_0(\alpha))^{\frac{n}{2}}}{n!} t^{\frac{n\alpha}{2}} E^{\frac{-n}{2}}_{1,1-\frac{n\alpha}{2}} \left(-\frac{k_1(\alpha)}{k_0(\alpha)} t\right),$$

$$u_4(\phi, t) = L^{-1}\{\bar{u}_4(\phi, s)\}$$

$$= L^{-1}\left\{\frac{1}{s^{\alpha}\left[\frac{k_1(\alpha)}{s} + k_0(\alpha)\right]}\right\}$$

$$= \frac{1}{k_0(\alpha)} t^{\alpha-1} E_{1,\alpha}\left(-\frac{k_1(\alpha)}{k_0(\alpha)} t\right).$$

In the case of $Gm = 0$, the solution for the velocity field becomes

$$\begin{aligned} u(\phi, t) = & \sum_{n=0}^{\infty} \frac{(-\phi)^n (\lambda k_0(\alpha))^{\frac{n}{2}}}{n!} t^{\frac{n\alpha}{2}} E^{\frac{-n}{2}}_{1,1-\frac{n\alpha}{2}} \left(-\frac{k_1(\alpha)}{k_0(\alpha)} t\right) \\ & + \left(\frac{\lambda Gr}{\lambda - Pr_0}\right)\left[\frac{1}{k_0(\alpha)} t^{\alpha-1} E_{1,\alpha}\left(-\frac{k_1(\alpha)}{k_0(\alpha)} t\right)\right] * \left[\sum_{n=0}^{\infty} \frac{(-\phi)^n (Pr_0 k_0(\alpha))^{\frac{n}{2}}}{n!} t^{\frac{n\alpha}{2}} E^{\frac{-n}{2}}_{1,1-\frac{n\alpha}{2}} \left(-\frac{k_1(\alpha)}{k_0(\alpha)} t\right)\right] \\ & - \left(\frac{\lambda Gr}{\lambda - Pr_0}\right)\left[\frac{1}{k_0(\alpha)} t^{\alpha-1} E_{1,\alpha}\left(-\frac{k_1(\alpha)}{k_0(\alpha)} t\right)\right] * \left[\sum_{n=0}^{\infty} \frac{(-\phi)^n (\lambda k_0(\alpha))^{\frac{n}{2}}}{n!} t^{\frac{n\alpha}{2}} E^{\frac{-n}{2}}_{1,1-\frac{n\alpha}{2}} \left(-\frac{k_1(\alpha)}{k_0(\alpha)} t\right)\right] \\ & + \left(\frac{\lambda Gm}{\lambda - Sc}\right)\left[\frac{1}{k_0(\alpha)} t^{\alpha-1} E_{1,\alpha}\left(-\frac{k_1(\alpha)}{k_0(\alpha)} t\right)\right] * \left[\sum_{n=0}^{\infty} \frac{(-\phi)^n (Sc k_0(\alpha))^{\frac{n}{2}}}{n!} t^{\frac{n\alpha}{2}} E^{\frac{-n}{2}}_{1,1-\frac{n\alpha}{2}} \left(-\frac{k_1(\alpha)}{k_0(\alpha)} t\right)\right] \\ & - \left(\frac{\lambda Gm}{\lambda - Sc}\right)\left[\frac{1}{k_0(\alpha)} t^{\alpha-1} E_{1,\alpha}\left(-\frac{k_1(\alpha)}{k_0(\alpha)} t\right)\right] * \left[\sum_{n=0}^{\infty} \frac{(-\phi)^n (\lambda k_0(\alpha))^{\frac{n}{2}}}{n!} t^{\frac{n\alpha}{2}} E^{\frac{-n}{2}}_{1,1-\frac{n\alpha}{2}} \left(-\frac{k_1(\alpha)}{k_0(\alpha)} t\right)\right]. \end{aligned} \tag{5.4}$$

6. Results and discussion

The present work examines the analytical solutions of the mathematical fractional Casson fluid model for flow through porous plate near an infinitely vertical plate, saturated in porous medium. The phenomenon has been expressed in terms of partial differential equations, and the governing equations have been transformed in non-dimensional form with suitable new non-dimensional variables. For the sake of better rheology of Casson fluid, we developed a fractional model by employing the new definition of the Constant Proportional Caputo fractional derivative operator having non-local and singularized kernel that describes the generalized memory effects. For seeking exact solution expressions in terms of Mittag-Leffler functions, for Casson fluid velocity, concentration and Casson fluid temperature, the Laplace integral transformation method is used to solve the fractional model. The physical significance of various system parameters involved in the problem, such as fractional parameter α, thermal Grashof number Gr, Casson fluid parameter β, Prandtl number Pr, Schmidt number Sc and mass Grashof number Gm, on the Casson fluid velocity, concentration and Casson fluid temperature are evaluated graphically in Figures 2–11 by using graphical Mathcad Software. A new aspect of this presented work is the use of the Constant Proportional Caputo fractional operator for Casson fluid with symmetry boundary conditions.

Figure 2 portrays the impact of fractional parameter α on fluid temperature and concentration against ϕ, and a significant effect on fluid temperature within the boundary layer is investigated. For

distinct values of fractional parameter, increasing values of α, and consequently, temperature and concentration profiles are decreased.

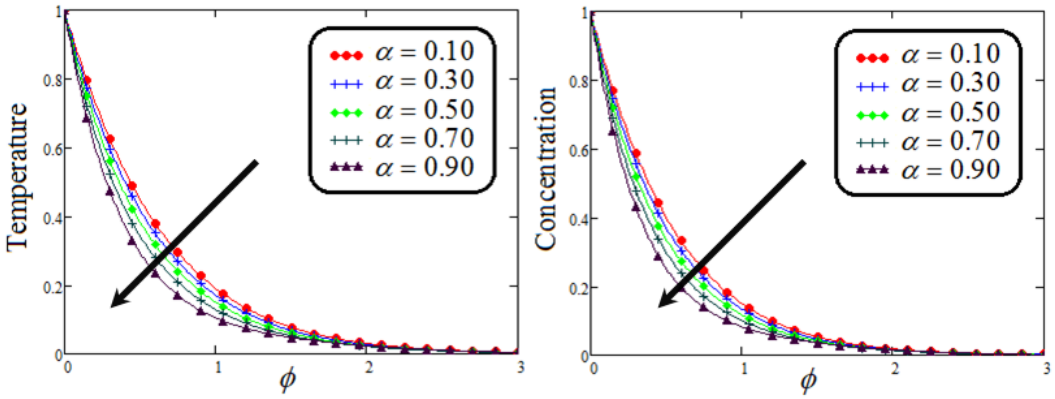

Figure 2. Simulation to illustrate the temperature and concentration profiles for distinct values of the fractional parameter α.

Figure 3 displays the Prandtl number P_r effect on Casson fluid temperature distribution against ϕ, for different values of P_r, at four different values of fractional parameter α. It is noticed that a decreasing effect on temperature in the boundary layer occurred when the values of the Prandtl number enlarged. Physically, increasing the values of Prandtl number increases the fluid viscosity, so the fluid becomes thicker, and as a result, fluid temperature decreased.

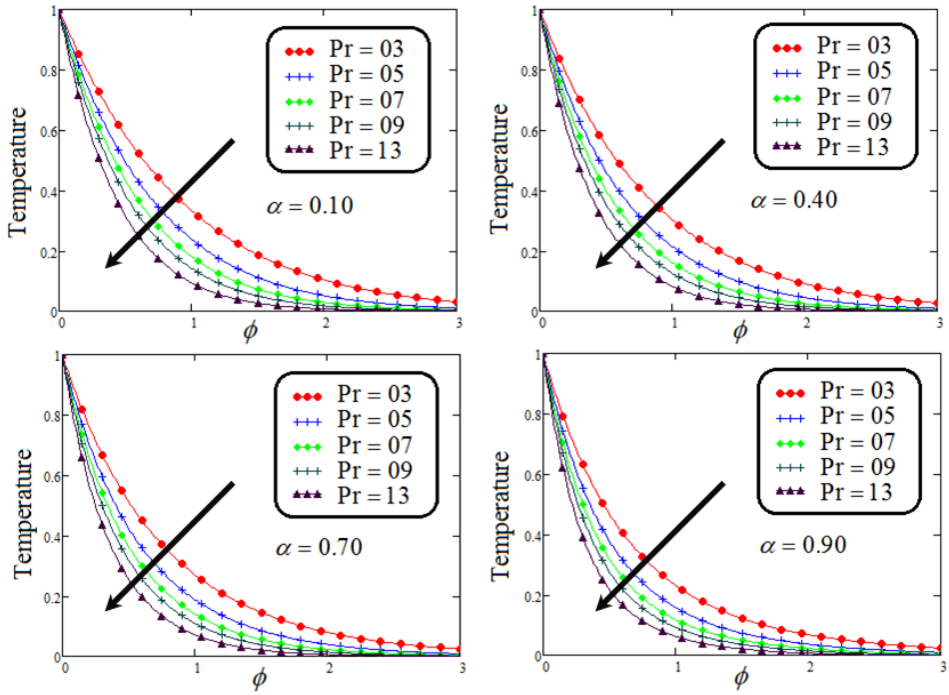

Figure 3. Simulation to illustrate the temperature profile for varying the values of Pr at distinct values of the fractional parameter α.

Figure 4 illustrates the effect of Sc on concentration profile of Casson fluid by changing its value. From the curves, it is analysed that concentration profile reduced for large values of Sc, where the values of fractional parameters have been considered between 0 and 1. Physically, boundary layer of concentration is declined due to change of Schmidt number from small to large. Figure 5 depicts the graphical behaviour of fractional parameter α, and a significant effect is noticed on Casson fluid velocity curve together with system parameters. It is noteworthy that the curves of the fluid velocity for small values of fractional parameter is lower, and the curves of fluid velocity increased continuously corresponding to increasing values of fractional parameter. Figure 6 represents the behaviour of Casson fluid parameter β to analyse its effect on velocity contours, and variation of velocity field against ϕ under the influence of Casson parameter β is noticed in this graph together with the involved parameters. It is observed that they share an inverse relation, as an increase in β results in flow retardation. The physical phenomenon causing this retardation is the plasticity of fluid. When parameter β reduces, momentum boundary layer thickness increases due to an increase in the plasticity of the fluid. With increasing values of Casson fluid parameter, the velocity graphs are reduced as a result. Also, it is analysed from the graph of fluid velocity that the momentum boundary layer thickness reduced corresponding to increasing the values of Casson fluid parameter. Furthermore, the non-Newtonian fluid behaviour fully vanishes, when the value of Casson parameter is very very large $(\frac{1}{\beta}) \to 0$, then in this case fluid totally changed in viscous fluid. From these results, it is concluded that the thickness of velocity boundary layer is larger for Newtonian fluid as compared to the Casson fluid.

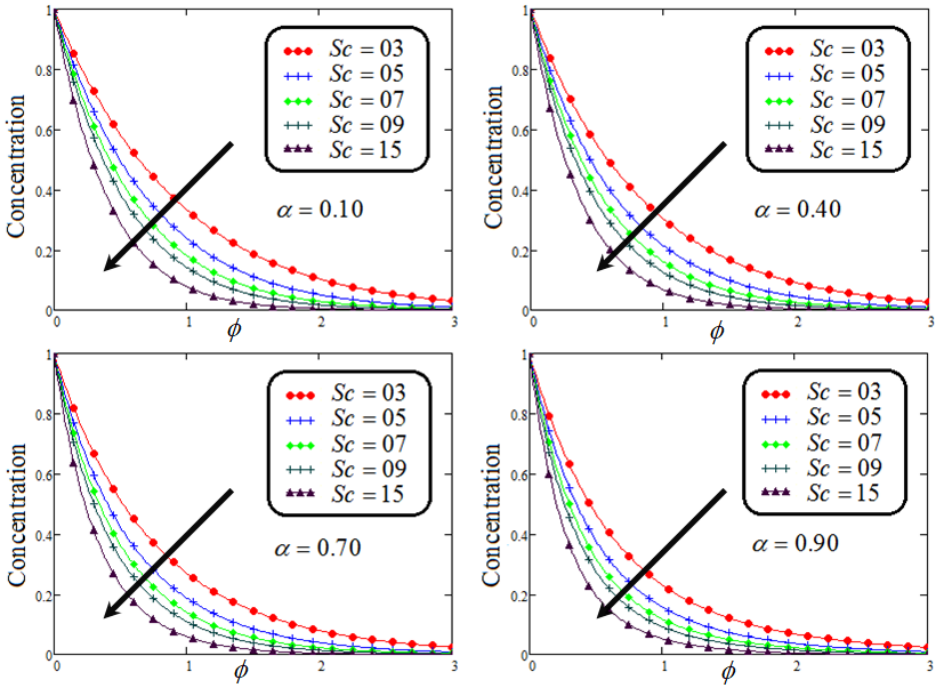

Figure 4. Representation of concentration profile against ϕ for distinct values of Sc for distinct values of the fractional parameter α.

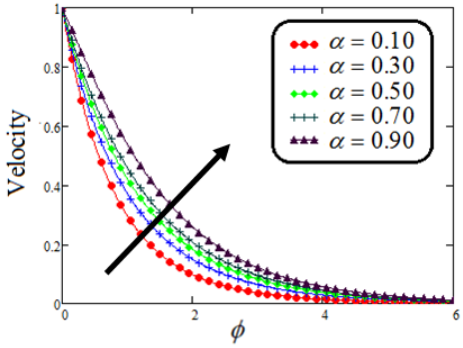

Figure 5. Representation of Casson fluid velocity against ϕ for distinct values of α.

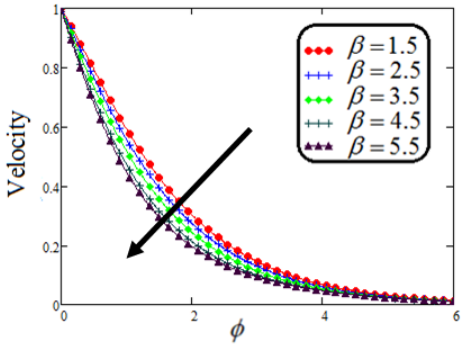

Figure 6. Representation of Casson fluid velocity against ϕ for distinct values of β.

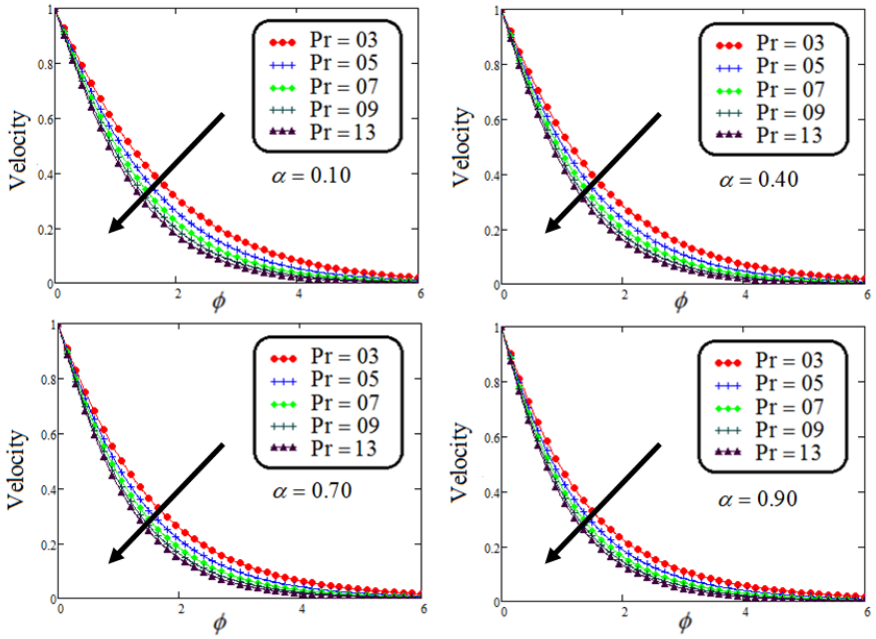

Figure 7. Representation of Casson fluid velocity against ϕ for distinct values of Pr.

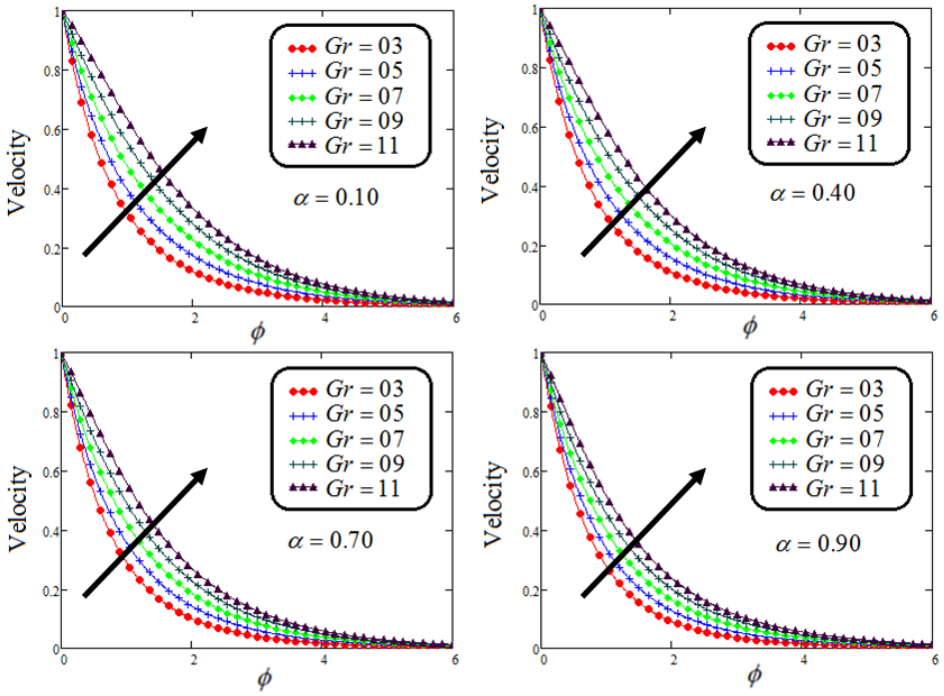

Figure 8. Representation of Casson fluid velocity against ϕ for distinct values of Gr.

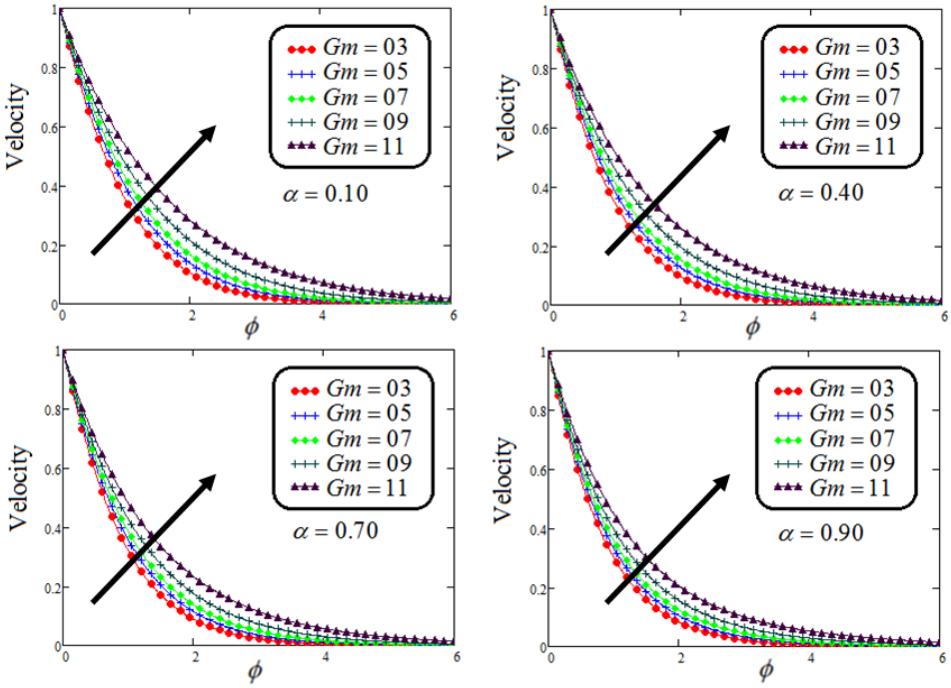

Figure 9. Representation of Casson fluid velocity against ϕ for distinct values of Gm.

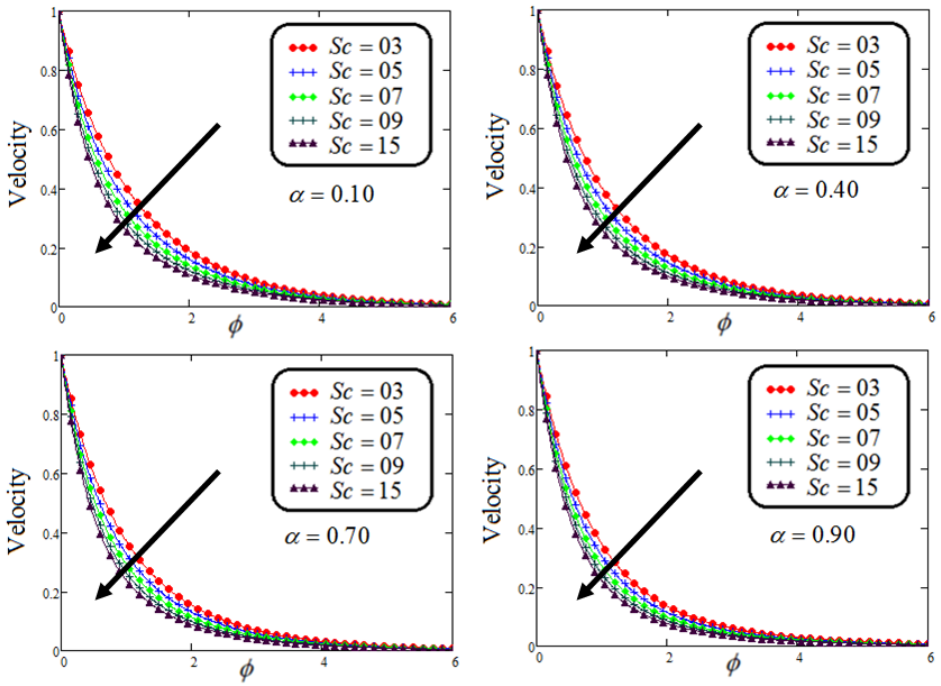

Figure 10. Representation of Casson fluid velocity against ϕ for distinct values of Sc.

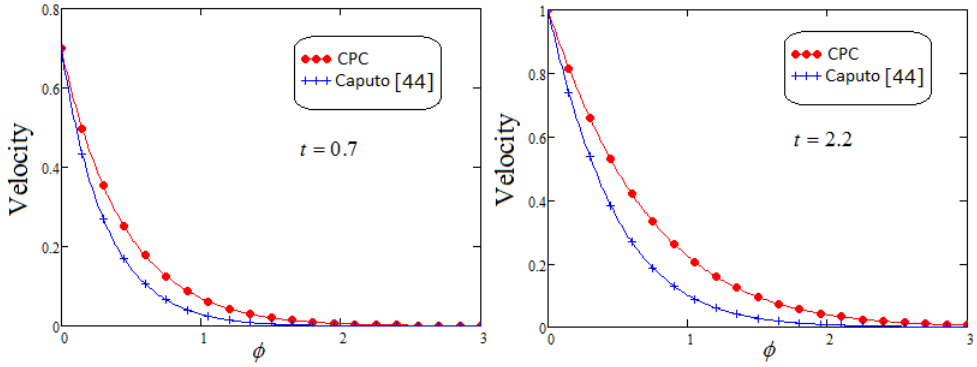

Figure 11. Comparison of CPC fractional operator and Caputo fractional operator against ϕ.

Figure 7 exhibits the effect of Prandtl number P_r on Casson fluid velocity corresponding to ϕ, for different values of P_r, at four different values of fractional parameter α. There was a decreasing effect on velocity in the boundary layer when the values of the Prandtl number enlarged. Physically, an increased Prandtl number causes an increased fluid viscosity. Because of this, the fluid becomes thicker, and as a result, fluid velocity decreased. Figures 8 and 9 portrays the influence of thermal Grashof numbers Gr and mass Grashof number Gm on Casson fluid flow against ϕ. Gr describes the fraction of thermal buoyancy force to viscous force and Gm describes the fraction of species buoyancy force to viscous force acting on the fluid transportation. As a result, increasing Gr or Gm causes a remarkable increasing impact on the Casson fluid velocity. Physically, increasing values of thermal or mass Grashof numbers leads to decreases in viscous hydrodynamic forces, and as a result, the

momentum of the Casson fluid is higher.

Figure 10 the effect of Sc on Casson fluid velocity curve is depicted, against ϕ, for different values of Sc, at four different values of fractional parameter α. There was a decreasing effect on velocity contour when the values of the Schmidt number enlarged. Physically, the relative influence of momentum diffusivity to species diffusivity is the definition of Schmidt number Sc. It is noticed that, momentum diffusivity is quicker than species diffusivity when Sc is greater than one ($Sc > 1$), but it is the reverse when Sc is less than one ($Sc < 1$). In the case of ($Sc = 1$), both species and momentum boundary layers have magnitude of the same order. Figure 11 gives a comparative illustration of velocity field for Constant Proportional Caputo and Caputo fractional operators. It also shows the velocity profile at two different levels of time, and it is witnessed that the CPC time fractional operator produces the higher velocity profile as compared to the Caputo fractional model.

7. Conclusions

In this article, the analytical solutions of the mathematical fractional Casson fluid that flows through vertical porous plate under symmetry boundary conditions is investigated. The phenomenon has been expressed in terms of partial differential equations, and then the governing equations were transformed in non-dimensional form. For the sake of better rheology of Casson fluid, we developed a fractional model by employing the new definition of Constant Proportional Caputo hybrid fractional operator that describes the generalized memory effects. For seeking exact solution expressions in terms of Mittag-Leffler functions, for Casson fluid velocity, concentration and Casson fluid temperature, the Laplace integral transformation method is used to solve the fractional model. For physical significance of several involved parameters, the graphical representations of the analytical solutions illustrated the main results of the present work. Also, from the literature, it is observed that deriving analytical results from fractional fluid models developed by the various fractional operators is difficult, and this article contributes to answering the open problem of obtaining analytical solutions of the fractionalized fluid models. Some noteworthy observations and concluding remarks are given below:

- It is detected that the fluid temperature is reduced when increasing the values of Pr. Also, reduction is observed in concentration profile for elevating the values of Sc for varying the values of fractional parameter (α).
- An increase in the values of Pr and Sc causes a decline in the velocity profile.
- The growing values of Gr and Gm increase the velocity field.
- Fluid temperature and concentration are decreasing functions of the fractional parameter α.
- Increasing values of α increase the momentum profile.
- It is observed that when elevating the Casson parameter β, the velocity graphs decreased.
- It can be noticed that the Casson fluid velocity displays the same behaviour for small and large values of α.

Future researchers can investigate the same problem by employing various fractional derivative operators having singular and non-singular kernels.

Conflict of interest

All the authors affirmed that they have no conflicts of interest.

References

1. M. Kahshan, D. Lu, A. M. Siddiqui, A Jeffrey fluid model for a porous-walled channel: application to flat plate dialyzer, *Sci. Rep.*, **9** (2019), 15879. https://doi.org/10.1038/s41598-019-52346-8
2. R. Mohebbi, A. A. Delouei, A. Jamali, M. Izadi, A. A. Mohamad, Pore-scale simulation of non-Newtonian power-law fluid flow and forced convection in partially porous media: thermal lattice Boltzmann method, *Phys. A.*, **525** (2019), 642–656. https://doi.org/10.1016/j.physa.2019.03.039
3. A. U. Rehman, M. B. Riaz, S. T. Saeed, S. Yao, Dynamical analysis of radiation and heat transfer on MHD second grade fluid, *Comp. Model. Eng. Sci.*, **129** (2021), 689–703. https://doi.org/10.32604/cmes.2021.014980
4. M. B. Riaz, K. A. Abro, K. M. Abualnaja, A. Akgül, A. U. Rehman, M. Abbas, et al., Exact solutions involving special functions for unsteady convective flow of magnetohydrodynamic second grade fluid with ramped conditions, *Adv. Differ. Equ.*, **2021** (2021), 408. https://doi.org/10.1186/s13662-021-03562-y
5. M. B. Riaz, J. Awrejcewicz, A. U. Rehman, Functional effects of permeability on Oldroyd-B fluid under magnetization: a comparison of slipping and non-slipping solutions, *Appl. Sci.*, **11** (2021), 11477. https://doi.org/10.3390/app112311477
6. Z. Khan, N. Tairan, W. K. Mashwani, H. U. Rasheed, H. Shah, W. Khan, MHD and slip effect on two-immiscible third grade fluid on thin film flow over a vertical moving belt, *Open Phys.*, **17** (2019), 575–586. https://doi.org/10.1515/phys-2019-0059
7. N. Casson, A flow equation for pigment-oil suspensions of the printing ink type, In: *Rheology of disperse systems*, Pergamon Press, 1959, 84–104.
8. R. K. Dash, K. N. Mehta, G. Jayaraman, Casson fluid flow in a pipe filled with a homogeneous porous medium, *Int. J. Eng. Sci.*, **34** (1996), 1145–1156. https://doi.org/10.1016/0020-7225(96)00012-2
9. Y. C. Fung, *Biodynamics*, Circulation, New York: Springer-Verlag, 1984. https://doi.org/10.1007/978-1-4757-3884-1
10. A. Khalid, I. Khan, A. Khan, S. Shafie, Unsteady MHD free convection flow of Casson fluid past over an oscillating vertical plate embedded in a porous medium, *Eng. Sci. Technol. Int. J.*, **18** (2015), 309–317. https://doi.org/10.1016/j.jestch.2014.12.006
11. K. Bhattacharyya, T. Hayat, A. Alsaedi, Analytic solution for magnetohydrodynamic boundary layer flow of Casson fluid over a stretching/shrinking sheet with wall mass transfer, *Chin. Phys. B*, **22** (2013), 024702. https://doi.org/10.1088/1674-1056/22/2/024702
12. S. Oka, An approach to α unified theory of the flow behaviour of time-independent non-Newtonian suspensions, *Jpn. J. Appl. Phys.*, **10** (1971), 287. https://doi.org/10.1143/JJAP.10.287
13. A. V. Mernone, J. N. Mazumdar, S. K. Lucas, A mathematical study of peristaltic transport of a Casson fluid, *Math. Comput. Model.*, **35** (2022), 895–912. https://doi.org/10.1016/S0895-7177(02)00058-4
14. E. M. Arthur, I. Y. Seini, L. B. Bortteir, Analysis of Casson fluid flow over a vertical porous surface with chemical reaction in the presence of magnetic field, *J. Appl. Math. Phys.*, **3** (2015), 713–723.

15. K. U. Rehman, E. A. Algehyne, F. Shahzad, E. M. Sherif, Y. M. Chu, On thermally corrugated porous enclosure (TCPE) equipped with Casson liquid suspension: finite element thermal analysis, *Case Stud. Therm. Eng.*, **25** (2021), 100873. https://doi.org/10.1016/j.csite.2021.100873

16. Q. Lou, B. Ali, S. U. Rehman, D. Habib, S. Abdal, N. A. Shah, et al., Micropolar dusty fluid: coriolis force effects on dynamics of MHD rotating fluid when Lorentz force is significant, *Mathematics*, **10** (2022), 2630. https://doi.org/10.3390/math10152630

17. M. Z. Ashraf, S. U. Rehman, S. Farid, A. K. Hussein, B. Ali, N. A. Shah, et al., Insight into significance of bioconvection on MHD tangent hyperbolic nanofluid flow of irregular thickness across a slender elastic surface, *Mathematics*, **10** (2022), 2592. https://doi.org/10.3390/math10152592

18. J. K. Madhukesh, R. N. Kumar, R. J. P. Gowda, B. C. Prasannkumara, G. K. Ramesh, M. I. Khan, et al., Numerical simulation of AA7072-AA7075/water-based hybrid nanofluid flow over a curved stretching sheet with Newtonian heating: a non-Fourier heat flux model approach, *J. Mol. Liq.*, **335** (2021), 116103. https://doi.org/10.1016/j.molliq.2021.116103

19. A. Bagh, S. Anum, S. Imran, A. Qasem, J. Fahd, Significance of suction/injection, gravity modulation, thermal radiation, and magnetohydrodynamic on dynamics of micropolar fluid subject to an inclined sheet via finite element approach, *Case Stud. Therm. Eng.*, **28** (2021), 101537. https://doi.org/10.1016/j.csite.2021.101537

20. Q. Raza, M. Z. A. Qureshi, B. A. Khan, A. K. Hussein, B. Ali, N. A. Shah, et al., Insight into dynamic of Mono and hybrid Nanofluids subject to binary chemical reaction, activation energy, and magnetic field through the porous surfaces, *Mathematics*, **10** (2022), 3013. https://doi.org/10.3390/math10163013

21. M. Mustafa, T. Hayat, I. Pop, A. Aziz, Unsteady boundary layer flow of a Casson fluid due to an impulsively started moving flat plate, *Heat Transf.*, **40** (2011), 563–576. https://doi.org/10.1002/htj.20358

22. A. Bagh, T. Thirupathi, H. Danial, S. Nadeem, R. Saleem, Finite element analysis on transient MHD 3D rotating flow of Maxwell and tangent hyperbolic nanofluid past a bidirectional stretching sheet with Cattaneo Christov heat flux model, *Case Stud. Therm. Eng.*, **28** (2022), 101089. https://doi.org/10.1016/j.tsep.2021.101089

23. M. Z. A. Qureshi, M. Faisal, Q. Raza, B. Ali, T. Botmart, N. A. Shah, Morphological nanolayer impact on hybrid nanofluids flow due to dispersion of polymer/CNT matrix nanocomposite material, *AIMS Math.*, **8** (2023), 633–656. https://doi.org/10.3934/math.2023030

24. B. Ali, S. Imran, A. Ali, S. Norazak, A. Liaqat, H. Amir, Significance of Lorentz and Coriolis forces on dynamics of water based silver tiny particles via finite element simulation, *Ain Sha. Eng. J.*, **13** (2022), 101572. https://doi.org/10.1016/j.asej.2021.08.014

25. S. Pramanik, Casson fluid flow and heat transfer past an exponentially porous stretching surface in presence of thermal radiation, *Ain Shams Eng. J.*, **5** (2014), 205–212. https://doi.org/10.1016/j.asej.2013.05.003

26. M. S. Osman, A. Korkmaz, H. Rezazadeh, M. Mirzazadeh, M. Eslami, Q. Zhou, The unified method for conformable time fractional Schrödinger equation with perturbation terms, *Chin. J. Phys.*, **56** (2018), 2500–2506. https://doi.org/10.1016/j.cjph.2018.06.009

27. M. Al-Smadi, A. Freihat, O. A. Arqub, N. Shawagfeh, A novel multistep generalized differential transform method for solving fractional-order Lu chaotic and hyperchaotic systems, *J. Comput. Anal. Appl.*, **19** (2015), 713–724.

28. S. Momani, A. Freihat, M. Al-Smadi, Analytical study of fractional-order multiple chaotic Fitzhugh-Nagumo neurons model using multistep generalized differential transform method, *Abstr. Appl. Anal.*, **2014** (2014), 276279. https://doi.org/10.1155/2014/276279

29. M. Alabedalhadi, M. Al-Smadi, S. Al-Omari, D. Baleanu, S. Momani, Structure of optical soliton solution for nonliear resonant space-time Schrödinger equation in conformable sense with full nonlinearity term, *Phys. Scr.*, **95** (2020), 105215. https://doi.org/10.1088/1402-4896/abb739

30. Z. Altawallbeh, M. Al-Smadi, I. Komashynska, A. Ateiwi, Numerical solutions of fractional systems of two-point BVPs by using the iterative reproducing kernel algorithm, *Ukr. Math. J.*, **70** (2018), 687–701.

31. M. Al-Smadi, N. Djeddi, S. Momani, S. Al-Omari, S. Araci, An attractive numerical algorithm for solving nonlinear Caputo-Fabrizio fractional Abel differential equation in a Hilbert space, *Adv. Differ. Equ.*, **2021** (2021), 271. https://doi.org/10.1186/s13662-021-03428-3

32. M. N. Islam, M. A. Akbar, Closed form exact solutions to the higher dimensional fractional Schrodinger equation via the modified simple equation method, *J. Appl. Math. Phys.*, **6** (2018), 90–102. https://doi.org/10.4236/jamp.2018.61009

33. M. Al-Smadi, O. A. Arqub, S. Hadid, Approximate solutions of nonlinear fractional Kundu-Eckhaus and coupled fractional massive Thirring equations emerging in quantum field theory using conformable residual power series method, *Phys. Scr.*, **95** (2020), 105205. https://doi.org/10.1088/1402-4896/abb420

34. M. Al-Smadi, O. A. Arqub, M. Gaith, Numerical simulation of telegraph and Cattaneo fractional-type models using adaptive reproducing kernel framework, *Math. Methods Appl. Sci.*, **44** (2021), 8472–8489. https://doi.org/10.1002/mma.6998

35. S. Momani, N. Djeddi, M. Al-Smadi, S. Al-Omari, Numerical investigation for Caputo-Fabrizio fractional Riccati and Bernoulli equations using iterative reproducing kernel method, *Appl. Numer. Math.*, **170** (2021), 418–434. https://doi.org/10.1016/j.apnum.2021.08.005

36. S. Hasan, M. Al-Smadi, A. El-Ajou, S. Momani, S. Hadid, Z. Al-Zhour, Numerical approach in the Hilbert space to solve a fuzzy Atangana-Baleanu fractional hybrid system, *Chaos Solitons Fract.*, **143** (2021), 110506. https://doi.org/10.1016/j.chaos.2020.110506

37. M. B. Riaz, J. Awrejcewicz, A. U. Rehman, M. Abbas, Special functions-based solutions of unsteady convective flow of a MHD Maxwell fluid for ramped wall temperature and velocity with concentration, *Adv. Differ. Equ.*, **2021** (2021), 500. https://doi.org/10.1186/s13662-021-03657-6

38. M. B. Riaz, J. Awrejcewicz, A. U. Rehman, A. Akgül, Thermophysical investigation of Oldroyd-b fluid with functional effects of permeability: memory effect study using non-singular kernel derivative approach, *Fractal Fract.*, **5** (2021), 124. https://doi.org/10.3390/fractalfract5030124

39. A. Atangana, D. Baleanu, New fractional derivative with non local and non-singular kernel: theory and application to heat transfer model, *Thermal Sci.*, **20** (2016), 763–769.

40. A. U. Rehman, J. Awrejcewicz, M. B. Riaz, F. Jarad, Mittag-Leffler form solutions of natural convection flow of second grade fluid with exponentially variable temperature and mass diffusion using Prabhakar fractional derivative, *Case Stud. Therm. Eng.*, **34** (2022), https://doi.org/10.1016/j.csite.2022.102018

41. M. B. Riaz, A. U. Rehman, J. Awrejcewicz, A. Akgül, Power law kernel analysis of MHD Maxwell fluid with ramped boundary conditions: transport phenomena solutions based on special functions, *Fractal Fract.*, **5** (2021), 248. https://doi.org/10.3390/fractalfract5040248

42. A. U. Rehman, M. B. Riaz, W. Rehman, J. Awrejcewicz, D. Baleanu, Fractional modeling of viscous fluid over a moveable inclined plate subject to exponential heating with singular and non-singular kernels, *Math. Comput. Appl.*, **27** (2022), 8. https://doi.org/10.3390/mca27010008

43. Y. M. Chu, R. Ali, M. I. Asjad, A. Ahmadian, N. Senu, Heat transfer flow of Maxwell hybrid nanofluids due to pressure gradient into rectangular region, *Sci. Rep.*, **10** (2020), 16643. https://doi.org/10.1038/s41598-020-73174-1

44. N. Sene, Analytical solutions of a class of fluids models with the Caputo fractional derivative, *Fractal Fract.*, **6** (2022), 35. https://doi.org/10.3390/ fractalfract6010035

45. T. Hayat, S. A. Shehzad, A. Alsaedi, M. S. Alhothuali, Mixed convection stagnation point flow of Casson fluid with convective boundary conditions, *Chin. Phys. Lett.*, **29** (2012), 114704. https://doi.org/10.1088/0256-307X/29/11/114704

46. K. B. Charyya, Boundary layer stagnation-point flow of Casson fluid and heat transfer towards a shrinking/stretching sheet, *Front. Heat Mass Tran.*, **4** (2013), 023003. http://dx.doi.org/10.5098/hmt.v4.2.3003

47. A. Khalid, I. Khan, A. Khan, S. Shafie, Unsteady MHD free convection flow of Casson fluid past over an oscillating vertical plate embedded in a porous medium, *Eng. Sci. Technol. Int. J.*, **18** (2015), 309–317. https://doi.org/10.1016/j.jestch.2014.12.006

48. M. Mustafa, J. A. Khan, Model for flow of Casson nanofluid past a non-linearly stretching sheet considering magnetic field effects, *AIP Adv.*, **5** (2015), 077148. https://doi.org/10.1063/1.4927449

49. D. Baleanu, A. Fernandez, A. Akgül, On a fractional operator combining Proportional and Classical Differintegrals, *Mathematics*, **8** (2020), 360. https://doi.org/10.3390/math8030360